AEM
Journals.ASM.org

Stratified Microbial Structure and Activity in Sulfide- and Methane-Producing Anaerobic Sewer Biofilms

Jing Sun,[a] Shihu Hu,[a] Keshab Raj Sharma,[a,b] Bing-Jie Ni,[a] Zhiguo Yuan[a,b]

Advanced Water Management Centre, The University of Queensland, St. Lucia, Queensland, Australia[a]; CRC for Water Sensitive Cities, Clayton, Victoria, Australia[b]

Simultaneous production of sulfide and methane by anaerobic sewer biofilms has recently been observed, suggesting that sulfate-reducing bacteria (SRB) and methanogenic archaea (MA), microorganisms known to compete for the same substrates, can coexist in this environment. This study investigated the community structures and activities of SRB and MA in anaerobic sewer biofilms (average thickness of 800 μm) using a combination of microelectrode measurements, molecular techniques, and mathematical modeling. It was seen that sulfide was mainly produced in the outer layer of the biofilm, between the depths of 0 and 300 μm, which is in good agreement with the distribution of SRB population as revealed by cryosection-fluorescence *in situ* hybridization (FISH). SRB had a higher relative abundance of 20% on the surface layer, which decreased gradually to below 3% at a depth of 400 μm. In contrast, MA mainly inhabited the inner layer of the biofilm. Their relative abundances increased from 10% to 75% at depths of 200 μm and 700 μm, respectively, from the biofilm surface layer. High-throughput pyrosequencing of 16S rRNA amplicons showed that SRB in the biofilm were mainly affiliated with five genera, *Desulfobulbus*, *Desulfomicrobium*, *Desulfovibrio*, *Desulfatiferula*, and *Desulforegula*, while about 90% of the MA population belonged to the genus *Methanosaeta*. The spatial organizations of SRB and MA revealed by pyrosequencing were consistent with the FISH results. A biofilm model was constructed to simulate the SRB and MA distributions in the anaerobic sewer biofilm. The good fit between model predictions and the experimental data indicate that the coexistence and spatial structure of SRB and MA in the biofilm resulted from the microbial types and their metabolic transformations and interactions with substrates.

Sewer biofilms comprise complex multispecies microflora with a typical thickness of only about 1 mm (1). Depending on the electron donors and electron acceptors present in the wastewater, different carbon transformation processes can occur in close proximity in the sewer biofilms. Domestic wastewater normally contains a significant concentration (ca. 100 to 1,000 μM) of sulfate but negligible nitrite and nitrate concentrations (2, 3). Therefore, under anaerobic conditions (which normally occur in pressure sewers fully filled with wastewater), sulfate reduction carried out by sulfate-reducing bacteria (SRB) could be an important terminal electron-accepting process in the sewer biofilms. The sulfate reduction activity in anaerobic sewers is important, as the production of sulfide can be transferred to the gas phase of partially filled gravity sewers and cause extensive corrosion of concrete sewer pipes (4, 5). Also, the emission of sulfide from sewers can cause odor problems for the surrounding area and pose health risks to sewer workers (6, 7). Apart from sulfate reduction, methanogenesis caused by the respiration of methanogenic archaea (MA) could also be a key terminal process in anaerobic sewer biofilms (8, 9). Guisasola and colleagues found that methanogenesis accounted for more than 70% of the chemical oxygen demand (COD) loss in laboratory anaerobic sewer biofilm reactors (9). A recent report suggests that methane emissions from sewers contribute significantly to the total greenhouse gas footprint of wastewater systems (10).

Under anaerobic conditions, both sulfate reduction and methanogenesis can potentially occur in the same system while competing for the same electron donors, primarily, hydrogen and acetate. In the presence of adequate sulfate concentrations, SRB typically out-compete MA due to kinetic and thermodynamic advantages (11–13). However, the coexistence of SRB and MA has been observed in anaerobic sewer biofilms in the presence of sulfate. Guisasola et al. (9) hypothesized that the coexistence of SRB and MA in sewer biofilms was due to the penetration limitation of sulfate into the biofilms, resulting in a stratified biofilm structure, with SRB being predominant in the outer zone, nearer the wastewater, while MA inhabit the inner zone, nearer the sewer pipe. However, to date this hypothesis has not been verified. A few studies have investigated the vertical distribution of SRB in oxic-anoxic sewer biofilms (biofilms attached to gravity sewer pipe with the presence of oxygen or nitrate in wastewater), but studies on the SRB distribution in the anaerobic sewer biofilms are scarce (14). In addition, the distribution of MA in sewer biofilms and their interaction with SRB have not yet been explored. Similarly, the phylogenetic diversity of SRB and MA in the anaerobic sewer biofilms has rarely been reported. This fundamental information could provide a better understanding of the sulfate reduction and methanogenesis processes in sewer systems, which would be useful for sewer management. Therefore, the aims of this study were to investigate the community structures of both SRB and MA and to determine their spatial arrangement in anaerobic sewer biofilms.

Both experimental investigations and modeling analyses were conducted to achieve the aims of this study. The experiments were carried out in an annular biofilm reactor fed with real domestic

Received 13 July 2014 **Accepted** 2 September 2014
Published ahead of print 5 September 2014
Editor: G. Voordouw
Address correspondence to Zhiguo Yuan, zhiguo@awmc.uq.edu.au.
Supplemental material for this article may be found at http://dx.doi.org/10.1128/AEM.02146-14.

doi:10.1128/AEM.02146-14

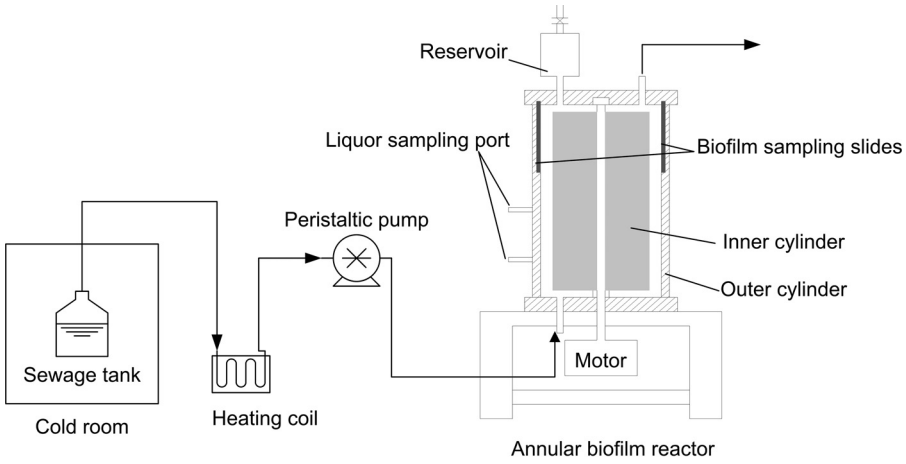

FIG 1 Schematic of the laboratory-scale anaerobic, annular biofilm reactor.

wastewater, mimicking anaerobic sewer conditions. First, microelectrodes were applied to determine the spatial distribution of *in situ* sulfide production activity within the biofilms. Although it would have been ideal to determine the distribution of methane production activity using the same method, this was difficult to perform due to the lack of suitable microelectrodes (15). Second, the spatial distributions of the SRB and MA in the biofilms and their abundances at different depths were determined by fluorescence *in situ* hybridization (FISH) after cryosectioning of the biofilm samples. This method has been used frequently to determine the spatial distributions of microbial communities in biofilms or granules. However, little phylogenetic information is revealed due to the limitations of the oligonucleotide probes used in FISH (16). Therefore, 16S rRNA gene amplicon pyrosequencing was applied to further investigate the phylogenetic diversity. In previous studies of sewer biofilms, the phylogenetic analysis was performed on the entire biofilm, and information on the different genera at different biofilm depths has rarely been reported (2, 14). In this study, we determined the phylogenetic diversity in different layers of the sewer biofilms by innovatively using pyrosequencing combined with cryosectioning. To our knowledge, to date, this method has not been applied in any other studies related to biofilms and granules. Finally, a mathematical model focusing on the interaction between SRB and MA in the sewer biofilm was developed to evaluate and interpret the experimental results.

MATERIALS AND METHODS

Reactor configuration, operation, and monitoring. An annular biofilm reactor made of acrylonitrile butadiene styrene (ABS), one of the typical materials used for sewer pipes, was set up to mimic an anaerobic sewer pipe section (Fig. 1). The reactor consisted of an inner cylinder (height, 295 mm; diameter, 130 mm) enclosed in an outer cylinder (height, 345 mm; diameter, 160 mm). The gap between the two cylinders was filled with wastewater (volume, 3 liters). Biofilms were grown on the walls of both cylinders in contact with the wastewater, resulting in a biofilm-area-to-reactor-volume (A/V) ratio of 119 m^{-1}. Mixing was established by the rotation of the inner cylinder driven by a motor at a speed of 200 rpm. The mixing was expected to create a uniform shear stress on the reactor walls to ensure that biofilms grew relatively evenly on the wall. The average shear stress provided by the mixing was 2.11 N/m^2, which is typical in sewer systems (17). Eight removable ABS slides of 5-mm width and 200-mm length were mounted in recessed slots inside the outer cylinder. The slides were removable via ports on the top of the reactor for biofilm sampling. The reservoir on the top of the reactor was used to ensure that the reactor was full of wastewater during sampling. The reactor was operated in a temperature-controlled room (20 ± 2°C). Domestic sewage, collected on a weekly basis from a local wet well (Brisbane, Queensland), was used as the feed for the reactor. The sewage compositions varied to a certain extent in terms of sulfate, volatile fatty acid (VFA), and COD concentrations. The sewage typically contained sulfate at concentrations of 10 to 25 mg S/liter, sulfide at <3 mg S/liter, soluble COD (sCOD) at 200 to 300 mg/liter, 50 to 120 mg COD/liter of VFAs, and approximately 50 mg N/liter of ammonium. Negligible amounts of sulfite, thiosulfate (<1 mg S/liter), nitrate, and nitrite (<1 mg N/liter) were present. The sewage was stored in a cold room (4°C) to minimize biological transformation and was heated to 20 ± 1°C prior to being pumped into the reactor (Fig. 1), which was consistent with the ambient temperature.

The sewage was fed to the reactor intermittently by a peristaltic pump (Masterflex 7520-47) to simulate the typical flow patterns of rising main sewers (main pressure sewers). For easier reactor monitoring, each day was divided into three identical 8-h periods. Figure S1 in the supplemental material shows the pumping patterns applied to the reactor for an 8-h period and the hydraulic retention time (HRT) (a measure of the average length of time that a soluble compound remains in a constructed bioreactor) of sewage in the reactor. Every pumping event lasted for 3 min, delivering one reactor volume (3 liters) of wastewater into the reactor. The HRTs of the wastewater ranged between 30 min and 4 h, which are in the range of the HRTs observed in a typical real sewer pipe (9).

Monitoring of the reactor performance was carried out during the 8-h cycle periods every 2 weeks. Sulfide concentrations during the 8-h cycle were continuously monitored using an S::CAN UV-visible light (UV-VIS) sepcitro::lyser (Messtechnik GmbH, Austria), as previously described by Sutherland-Stacey et al. (18). In addition, samples were taken from the reactor before and after each pumping event and also at 2.5 h, 5 h, and 6.5 h for the analysis of dissolved methane, sulfate, total COD (tCOD), sCOD, and VFAs, using methods described by Jiang et al. (3). Briefly, dissolved methane and VFA concentrations were measured by gas chromatography. Sulfate concentrations were measured using ion chromatography. tCOD and sCOD were determined by means of COD cuvette tests (Merck) (range, 25 to 1,500 mg $liter^{-1}$). Detailed studies of the biofilm were carried out when the reactor reached pseudo-steady-state conditions after about 10 months operation, as indicated by the relatively constant sulfide and methane profiles.

Microelectrode analyses. Hydrogen sulfide (i.e., molecular H_2S), pH, and dissolved oxygen levels in the biofilm were measured using microelectrodes (Unisense A/S; Denmark) with tip diameters of 10 μm, 25 μm,

and 100 μm, respectively. The sensors were calibrated according to the manufacturer's instructions. Hydrogen sulfide and pH profiles were measured to determine the total dissolved sulfide concentration as described by Kuhl et al. (19). Oxygen profiles were measured to confirm anaerobic conditions.

Before the microelectrode analyses, a length of about 5 cm of the biofilm slide was removed from the reactor and mounted in a flow cell (as described by Gutierrez et al. [20]) containing 140 ml of wastewater that had been filtered using a 0.22-μm-pore-size filter and 20 ml of 300 mM phosphate buffer (added to ensure a stable pH of 7.0 to 7.5). Nitrogen gas (99.99% purity) was bubbled through the flow cell to ensure anaerobic conditions and to provide mixing. Microelectrodes were mounted on a micromanipulator and positioned on the surface of the biofilm using a dissecting microscope. The concentration gradients through the biofilm were obtained by moving the microelectrodes in increments of 25 to 100 μm. Steady-state profiles were obtained by incubating the biofilm for 1 h in the medium before measurements were made.

The local sulfide production rates were calculated from the total sulfide profiles based on Fick's second law of diffusion. The calculation was carried out by a stepwise procedure as described by Gieseke and de Beer (21). Briefly, the production rate at point n can be calculated using following equations:

$$r_n = \frac{J_{n-1,n} - J_{n,n+1}}{0.5(x_{n-1} + x_n) - 0.5(x_n + x_{n+1})}$$

$$J_{n-1,n} = D_{\text{eff}} \frac{C_{n-1} - C_n}{x_{n-1} - x_n}, J_{n,n+1} = D_{\text{eff}} \frac{C_n - C_{n+1}}{x_n - x_{n+1}}$$

where $J_{n-1,n}$ and $J_{n,n+1}$ represent the flux between point $n-1$ and point n and the flux between point n and point $n+1$ (expressed in mol/m^2/s), x_{n-1}, x_n, and x_{n+1} represent the depths of points $n-1$, n, and $n+1$ (m), C_{n-1}, C_n, and C_{n+1} are sulfide concentrations at points $n-1$, n, and $n+1$ (mol/m^2), and D_{eff} represents the effective diffusion coefficient of sulfide in the biofilm (m^2/s). The value used in this study was 1.39×10^{-9} m^2/s (19), and this was based on the assumption that the diffusion coefficients within the biofilm were equal to the molecular diffusion coefficients.

Fluorescence *in situ* hybridization. Fluorescence *in situ* hybridization (FISH) was carried out to determine the distributions of SRB and MA in the biofilm. The sequences of all oligonucleotide probes used in this study are summarized in Table S1 in the supplemental material, and further detailed information is in probeBase (22). Due to a drawback of SRB probes, which can detect other bacteria that are not SRB, the SRB levels in this study were determined by the overlapping of the fluorescence signals of probes DELTA495a (CY3), DELTA495b (CY3), and DELTA495c (CY3) with those of probes SRB385 (CY5), SRB385Db (CY5), and DABAC 357 (CY5). Using this approach, most SRB in the phylum of the *Deltaproteobacteria* were detected while the non-SRB targeted by these probes were discriminated (16). SRB in other phyla were not detected by 16S rRNA pyrosequencing results, so probes for those phyla were not used. For FISH detection of MA, a combination of probes MSMX860 (CY5), MG1200b (CY5), MB1175 (CY5), MC1109 (CY5), and MC504 (CY5) was used to determine the total MA population in the biofilm. This combination of probes covers a wide range of MA in these ecosystems (23). SRB and MA levels were determined using different samples due to the different formamide concentrations required (35% for the SRB detection and 45% for the MA detection). Probes EUB338mix (fluorescein isothiocyanate [FITC]) and ARC915 (CY3) were used to determine all bacteria and archaea in the biofilm, respectively.

To conduct FISH analysis, the biofilm sampling slides were removed from the reactor and cut into sections with dimensions of approximately 10 mm by 5 mm. The biofilm samples on the small pieces were fixed with freshly prepared 4% paraformaldehyde solution for 2 h at 4°C. The fixed biofilm sample was then embedded in Tissue-Tek OCT compound (Sakura Finetek, Tokyo, Japan) following the procedures described by Batstone et al. (24). The biofilm samples were then allowed to settle on the base of the OCT molds and were frozen at −20°C. The frozen samples were then sectioned using a research cryostat (Leica CM3050 S) with a knife temperature of −20°C, a cabinet temperature of −18°C, and a section thickness of 10 μm. The samples were divided into two groups and cryosectioned in two different directions. One group of samples was sectioned perpendicularly to the substratum to provide sections to visualize the arrangement of SRB and MA distributed through the depth of the biofilm. The samples in the other group were successively sectioned parallel to the substratum from the surface to the bottom of the biofilm. These samples were used to determine the relative abundances of SRB and MA at eight different depths within the biofilm. The cryosectioned samples were placed on poly-L-lysine-coated microscope slides (Polysciences Asia Pacific, Inc.) and air dried for 6 to 10 h. The slides were then dehydrated for 3 min each (50%, 80%, and 98%) in an aqueous ethanol solution.

All *in situ* hybridizations were performed at 46°C for 2 to 3 h according to a previously described protocol (25) using hybridization buffer. The buffer contained 0.9 M NaCl, 20 mM Tris hydrochloride (pH 7.2), 0.01% sodium dodecyl sulfate, and formamide concentrations as previously mentioned. Subsequently, a stringent washing step was performed at 48°C for 15 min in 50 ml of washing solution comprising NaCl at a concentration dependent on the formamide concentration and 20 mM Tris hydrochloride at pH 7.2. The slides were examined and recorded using a Zeiss LSM 510 confocal laser scanning microscope (CLSM) (Carl Zeiss, Jena, Germany) and three excitation channels (488 nm, green emission; 545 nm, red emission; 633 nm, blue emission). The biofilm thickness was estimated by measuring the width of the biofilm sections cut perpendicularly to the substratum. FISH images at eight different depths of the biofilm (0 to 10 μm, 100 to 110 μm, 200 to 210 μm, 300 to 310 μm, 400 to 410 μm, 500 to 510 μm, 600 to 610 μm, and 700 to 710 μm) were analyzed using DAIME version 1.3 (26) to determine the biovolume fractions of SRB and MA. About 20 confocal images of the biofilm sections were analyzed for each sample. The quantification data were calculated based on the average results from two separately analyzed samples.

16S rRNA gene amplicon pyrosequencing. 16S rRNA gene amplicon pyrosequencing was conducted to investigate the phylogenetic diversity of SRB and MA at different layers in the biofilm. Biofilms on a piece of a slide (10 mm by 5 mm) were quickly removed from the reactor and embedded in OCT compound and then frozen at −20°C in a OCT mold. The frozen samples were then cryosectioned successively from the surface to the bottom of the biofilm with a section thickness of 150 μm, using the cryostat as described above. The sectioned biofilm samples were then placed separately in 1 ml Eppendorf tubes containing 0.5 ml of phosphate-buffered saline (PBS) (containing 137 mM NaCl, 2.7 mM KCl, 10 mM Na_2HPO_4, and 2 mM KH_2PO_4) for DNA extraction.

Genomic DNA was extracted using a FastDNA SPIN kit for soil according to the manufacturer's instructions (Q-Bio gene; Australia). The quantity and quality of the extracted DNA were measured using a NanoDrop ND-1000 spectrophotometer (Nano-Drop Technology, Rockland, DE) and agarose gel (0.8% [[wt/vol]) electrophoresis. Primers 926f (5′-AAACTYAAAKGAATTGACGG-3′) and 1392r (5′-ACGGGCGGTGTGTAC-3′) (27) containing multiplex identifiers and LibL adaptor sequences (not shown) were used to generate amplicons. The PCR tube (50 μl) contained 5 μl of 10× PCR buffer, 1 μl of 10 mM deoxynucleoside triphosphates (dNTPs), 1 μl (each) 10 mM primers, 4 μl of 25 mM $MgCl_2$, 1.5 μl of 10 mg/ml bovine serum albumin (BSA), 0.2 μl of 5.5 U/μl Fisher Biotec *Taq* DNA polymerase, and 2.5 μl of 20 ng/μl DNA sample. The PCR was conducted under the following conditions: 95°C for 3 min, followed by 30 cycles of 95°C for 30 s, 55°C for 30 s, and 74°C for 30 s and a final elongation step at 74°C for 10 min. The pyrosequencing of amplicons was carried out according to Roche 454 protocols using a Roche 454 GS FLX sequencer (Roche, Switzerland). The sequence data were analyzed through the use of the ACE Pyrosequencing Pipeline (https://github.com/minillinim/APP) in a local implementation. First, the sequencing reads were split according to the barcode in QIIME v1.8.0 (28). Then, demultiplexed sequences were trimmed to 250-bp lengths and denoised using

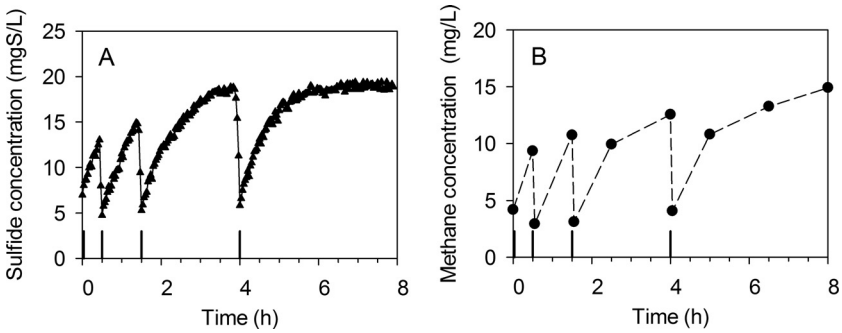

FIG 2 Sulfide (A) and methane (B) profiles in the sewer biofilm reactors during a typical 8-h cycle. The vertical solid lines at the bottom of the graphs indicate the pumping events in the 8-h cycle.

ACACIA (29). Sequences with 97% similarity were assigned to one operational taxonomic unit (OTU) by the use of CD-HIT-OTU (30) and aligned by Pynast (31). Each sequence was then assigned to the taxonomy with the BlastTaxonAssigner in QIIME through the greengenes database (August 2013 release). Sequences that were assigned to the classes of *Clostridia* and *Deltaproteobacteria* (containing most of the mesophilic SRB) and those assigned to the domain *Archaea* (containing the methanogens) were also compared with other sequences previously deposited in GenBank (http://www.ncbi.nlm.nih.gov) using the Basic Local Alignment Search Tool (BLAST), and genus-level classifications were assigned (in cases in which >98% identity was obtained). Finally, a nonnormalized OTU table was generated by QIIME. Then, Normalizer (https://github.com/minillinim/Normalizer) was used to construct a centroid normalized OTU table.

Biofilm modeling. A multispecies one-dimensional biofilm model was constructed to simulate the microbial structure and biological reactions in the anaerobic sewer biofilm, employing AQUASIM V2.1d software (32). The biofilm model was developed to evaluate the experimental results according to Sharma et al. (33) and Guisasola et al. (34). The biological reaction model is schematically summarized in Fig. S2 in the supplemental material, with definitions of model components summarized in Table S2.

Briefly, the biological model consisted of four types of microbial processes: hydrolysis, fermentation, sulfate reductions, and methanogenesis. Glucose was used in the reaction to represent fermentable substrates (e.g., sugars and/or other carbohydrates) in the same way it was used previously (34). Three fermentation products were considered in the model, namely, hydrogen, acetate, and propionate. Sulfate reductions were carried out with the three electron donors, i.e., hydrogen, acetate, and propionate. Given the fact that SRB tend to out-compete acetogenic bacteria for propionate utilization and that the propionate concentrations in real sewage were always lower than 10 mg COD/liter, propionate was considered an electron donor only for sulfate reduction (34). While sulfate reduction using fermentable substrates (e.g., sugars or other carbohydrates) is also possible, it was not considered in the model (34). The use of these substrates by SRB would otherwise be accounted for by the use of the fermentation products from these substrates. Both hydrogenotrophic and acetoclastic pathways for methanogenesis were included in the model. The stoichiometric matrix for microbial processes and the kinetic expressions of processes are shown in Table S3 and Table S4 in the supplemental material, respectively. All model parameters were obtained from the literature and are presented in Table S5.

Nucleotide sequence accession numbers. The 16S rRNA gene sequence data were deposited into the NCBI Short Read Archive (SRA) under accession numbers SRR1560806, SRR1560807, SRR1560808, SRR1560809, and SRR1560810.

RESULTS

Performance of the anaerobic sewer reactor. The typical sulfide and methane profiles in the sewer biofilm reactor during an 8-h operation cycle are shown in Fig. 2. Sulfide and methane were produced simultaneously in the reactor, and concentrations of sulfide (13.0 to 18.6 mg S/liter) and methane (9.3 to 14.9 mg/liter) at the end of each pumping cycle varied according to the HRT. During the 8-h cycle, the tCOD was decreased by 17% and nearly 86% of the sulfate was reduced. Table 1 shows the average daily transformation of COD, VFAs, sulfur species, and methane at the pseudo-steady state, calculated based on the concentration differences at the beginning and end of each pumping cycle. The tCOD was consumed by 688.2 ± 29.2 mg/day, with productions of sulfide and methane at 123.9 ± 11.1 mg S/day and 103.4 ± 3.2 mg/day, respectively. Similar daily sulfate consumption and sulfide production indicated that sulfide was the major product of sulfate reduction. The sCOD and propionate were also consumed in the reactor while acetate accumulated. The COD balance was calculated on the basis of the assumption that all of the hydrogen produced due to fermentation was consumed during the experiment. The COD utilization per gram of sulfide and methane formed was assumed to be 2 g COD/g H_2S-S and 4 g COD/g CH_4, respectively (9). Therefore, sulfidogenesis accounted for 36.0% ± 2.4% of the tCOD loss in the wastewater whereas methanogensis accounted for 60.0% ± 4.3% (Table 1).

Distribution of sulfide production within the biofilm. The microscale sulfide, pH, and oxygen levels were measured throughout the depth of the biofilm (Fig. 3). A significant increase of sulfide concentration is seen from the biofilm surface to ca. 250 μm into the biofilm. The pH remained constant throughout the depth of the biofilm, due to the buffering capacity of the system. Negligible levels of oxygen were detected within the biofilm. The *in situ* sulfide production rates were calculated based on the sulfide profiles according to Fick's law of diffusion (Fig. 3), which indi-

TABLE 1 Daily transformation of COD, VFAs, sulfur species, and methane in the sewer biofilm reactor

Compound	Unit	Daily transformation[a]	% ΔCOD
Total COD	mg COD	−688.2 ± 29.2	−100.0 ± 0.0
Soluble COD	mg COD	−362.5 ± 12.7	
Acetate	mg COD	+49.4 ± 17.2	
Propionate	mg COD	−76.5 ± 3.0	
Sulfate	mg S	−123.5 ± 12.8	
Sulfide	mg S	+123.9 ± 11.1	36.0 ± 2.4
Dissolved methane	mg	+103.4 ± 3.2	60.0 ± 4.3
COD balance			−4.0 ± 2.0

[a] +, production; −, consumption.

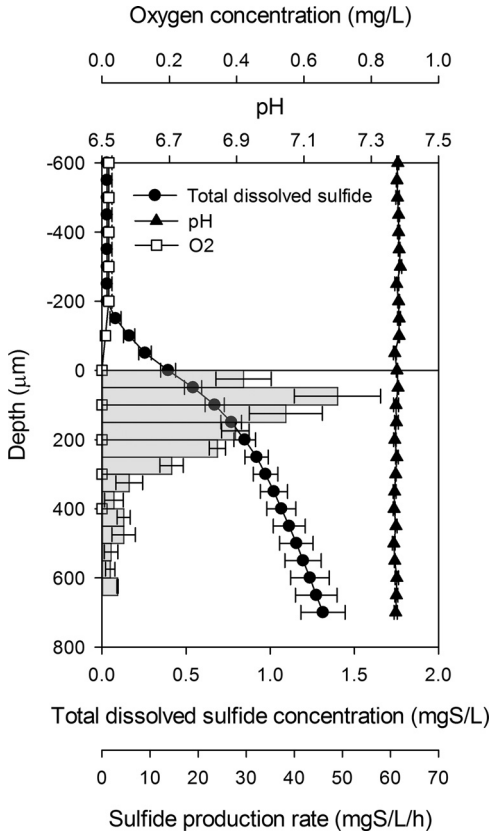

FIG 3 Profiles of measured total dissolved sulfide, oxygen, pH, and calculated sulfide production rate in the biofilm. Negative depths in the profile represent the distance from the biofilm surface into the wastewater.

cated that sulfide was mainly produced in the region that extended from the biofilm surface to a depth of about 300 μm into the biofilm. Though the sulfide concentration was highest below the depth of 300 μm, the calculated sulfide production under that depth accounted for only less than 10% of the total production.

Spatial distributions of SRB and MA populations as determined by FISH. FISH analysis of the biofilm sections cut perpendicularly to the substratum showed the localization of SRB and MA (Fig. 4A and B). SRB (white in Fig. 4A) were mainly situated at the outer layer (depth of 0 to 300 μm) of the biofilm, while MA (purple in Fig. 4B) were mainly located in the inner layer (below 250 μm). Panels C to F in Fig. 4 show typical FISH images of the biofilm sections cut parallel to the substratum at depths of 100 μm and 700 μm. Accordingly, SRB were detected in much higher abundance in the biofilm section at the depth of 100 μm than at the 700-μm-deep section (compare Fig. 4C to Fig. 4D). In contrast, there were hardly any MA at the depth of 100 μm whereas MA were dominant at the depth of 700 μm (compare Fig. 4E to Fig. 4F). The relative abundances of SRB and MA at different depths showed that SRB accounted for about 20% of the total population at the surface and at 100 μm into the biofilm and that the proportion decreased continuously to lower than 3% at the depth of 400 μm (Fig. 5). This distribution of SRB is consistent with the profile of the *in situ* sulfide production rate (Fig. 3). In contrast to the SRB distribution, the MA were detected at below 3% abundance at the surface and at the depth of 100 μm and increased in abundance to 10% at the depth of 200 μm, 60% at 500 μm, and then 75% at 700 μm (Fig. 5).

Biofilm community structure as determined by 16S rRNA sequence analysis. The 16S rRNA gene sequence analysis was successively applied to five layers of the biofilm, from the surface to the bottom of the biofilm (layer 1 to layer 5). The sequence reads for each layer are shown in Table S6 in the supplemental material. The thickness of each layer was 150 μm. The results revealed that the SRB detected in the biofilm were mainly affiliated with five genera and that their proportions of the total SRB detected were as follows: *Desulfobulbus* at 33%, *Desulfomicrobium* at 19%, *Desulfovibrio* at 24%, *Desulfatiferula* at 7%, and *Desulforegula* at 16%. The heat map (Fig. 6A) displaying the distributions of the predominant SRB in the different layers (layer 1 to layer 5) confirmed that SRB were mainly situated in the outer layer. SRB of the genera *Desulfobulbus*, *Desulfomicrobium*, and *Desulfovibrio* were also observed in inner layers 4 and 5, but the SRB in these inner layers accounted for only less than 10% of the total SRB detected in the biofilm. About 90% of the MA population belonged to the genus of *Methanosaeta*, whose members use acetate rather than hydrogen as the substrate. The other 10% of the MA population mainly belonged to five genera: *Methanospirillum*, *Methanomethylovorans*, *Methanobrevibacter*, *Methanobacterium*, and The heat map (Fig. 6B) also demonstrates that MA were mainly located in the inner layer of the biofilm. Interestingly, *Methanobrevibacter*, *Methanomethylovorans*, and *Methanospirillum* actually showed higher abundance in the outer layer than in the inner layer. However, these accounted for about 5% of the total MA population detected in the biofilm and thus had only a minor effect on the overall MA distribution in the biofilm.

Mathematical modeling. Mathematical modeling was performed to describe the microbial distribution and the sulfide concentration profiles within the biofilms. The model-predicted relative abundances of SRB and MA fit well with the experimental results determined by FISH (Fig. 7). The SRB abundance was 19% at the surface and decreased gradually to below 5% at the depth of 400 μm. The abundance of MA was lower than 5% at the surface and at 100 μm, increased to 65% at the depth of 500 μm, and then gradually rose to 80% at 700 μm. These results are consistent with the experimental data. The model-predicted sulfide concentration profiles within the biofilms also matched well with the data measured by microelectrode. The good agreement between the model-predicted results and the experimental data indicated that the spatial structure of SRB and MA in the anaerobic sewer biofilms resulted from the microbial types and their metabolic transformations and interactions with substrates.

DISCUSSION

The distribution of SRB and MA in anaerobic sewer biofilms. This study investigated the distribution of SRB and MA in sewer biofilms through both experimental analysis and simulation analysis. The stratified distribution of SRB and MA in the biofilm was confirmed and verified using two independent molecular techniques, i.e., FISH and pyrosequencing, as well as microelectrode measurements and mathematical modeling. All the results are highly consistent. The results show that SRB were mainly located in the outer layer of the biofilm whereas MA were mainly situated in the inner layer. The distribution of *in situ* sulfide production activity was consistent with the distribution of the SRB population. The high sulfide concentration in the inner layer of the bio-

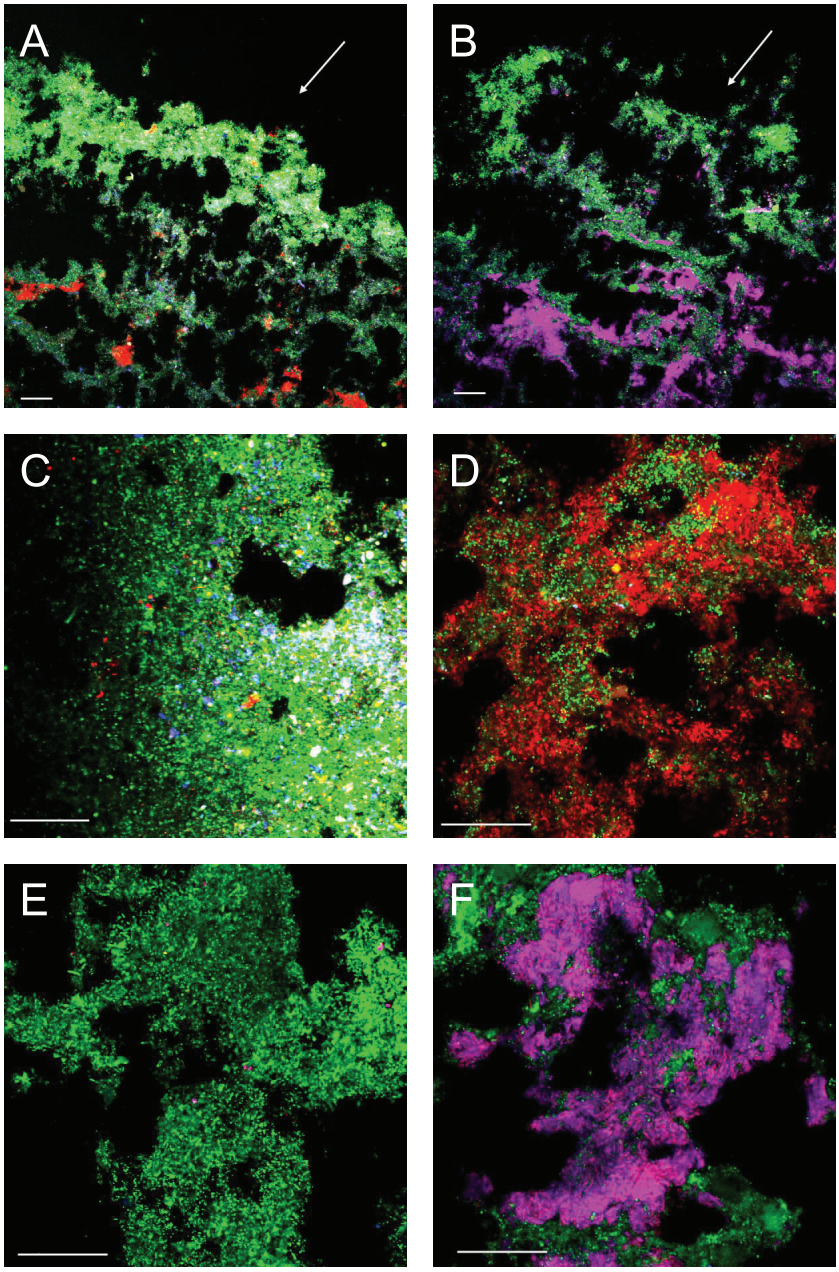

FIG 4 FISH images of different sections of the sewer reactor biofilm. (A and B) Images of the biofilm sections cut perpendicularly to the substratum, with SRB in white (A) and MA in purple (B). Arrows indicate the biofilm surface. (C and D) Images of biofilm sections cut parallel to the substratum at depths of 100 μm and 700 μm, respectively, with SRB in white, archaea in red, and other bacteria in green, blue, and yellow. (E and F) Images of biofilm sections cut parallel to the substratum at depths of 100 μm and 700 μm, respectively, with MA in purple, other archaea in red, and bacteria in green. Scale bars, 50 μm.

film was mainly due to the diffusion transport mechanism. While the sulfide production activity in the inner layer of the biofilm was much lower than that in the outer layer, in the absence of a sulfide sink in this layer, any sulfide produced would accumulate to a level higher than that accumulated in the outer layer, providing a concentration gradient for the sulfide produced to be transferred out of the biofilm.

Under anaerobic conditions, SRB and MA are known to compete for the same substrates (primarily acetate and hydrogen) for metabolism. In sulfate-rich environments, SRB can normally outcompete MA; this is commonly attributed to the different affinities of the two populations for substrates. The affinity constant for hydrogen of SRB is considered to be around five times lower than that of MA (35, 36). The difference is even greater in the case of acetate (12, 37). However, coexistence of SRB and MA is observed in some systems under sulfate-limiting conditions or even under non-sulfate-limiting conditions, where other factors play a role. These included mass transfer limitations (38) and differences in microbial colonization and adhesion properties (39, 40) or variable sulfide toxicities (41, 42).

In anaerobic sewers, particularly in networks with relatively short HRTs, sulfate is normally not depleted. The stratified distri-

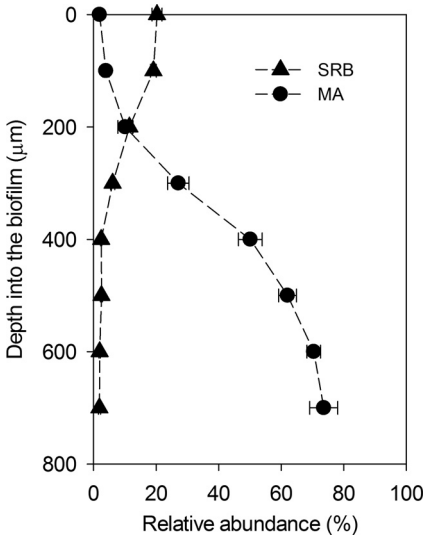

FIG 5 The SRB (A) and MA (B) proportions of total microorganisms (bacteria and archaea) detected by FISH within the sewer biofilms. *C. Methanomethylophilus*, "*Candidatus* Methanomethylophilus."

bution of SRB and MA suggests that mass transfer limitation plays an important role for the coexistence of SRB and MA in sewer biofilms. We used model simulation to determine the average concentrations of sulfate and soluble biodegradable COD in the sewer biofilm (Fig. 8). Sulfate could penetrate into the outer layer of the biofilm. Under these conditions, SRB out-competed MA due to their higher affinity to acetate and hydrogen, resulting in a higher abundance of SRB in the outer layer. However, the modeling result showed that the sulfate was almost totally consumed in the outer layer due to the high sulfate reduction activity and thus could not reach the inner layer (Fig. 8). As a result, SRB activity and growth were limited in the deeper layers of the biofilm. On the other hand, soluble biodegradable COD (including propionate, acetate, or hydrogen and the soluble COD which could be fermented to these products) was not totally consumed by SRB in the outer layer of the biofilm and it was able to penetrate into the inner layers, providing substrate for methanogenesis. Consequently, the coexistence and stratification of these populations are largely a result of the mass transfer of substrates into the biofilm.

The domination of MA in cores of anaerobic granules or at the inner layers of anaerobic biofilms has previously been attributed in some studies to better attachment characteristics of MA (40, 43). However, this cannot be a main reason in the case of anaerobic sewer biofilms. During the startup of the sewer reactor, the sulfate-reducing activity increased much faster than the methanogenic activity in the first several weeks (data not shown), indicating that at the beginning, more SRB were attached on the substratum than MA and that these were the pioneering colonizers of the biofilm. Variations of sulfide toxicities with respect to SRB and MA are also considered a reason for the coexistence of SRB and MA in some studies (41, 42). However, in our system, the sulfide concentration was far below toxic threshold levels for either group of microorganisms. It has been reported that sulfide concentrations of above 300 ppm are required to induce 50% inhibition of the growth of most SRB and MA (44).

The spatial arrangement of SRB and MA in sewer biofilms revealed in this study is of practical importance. Chemicals such as nitrate, oxygen, magnesium hydroxide, and sodium hydroxide are often added to sewers to control the emission of hydrogen sulfide in those sewers (6). As MA mainly inhabit the inner layer of the biofilms, they are likely to be protected from being exposed to

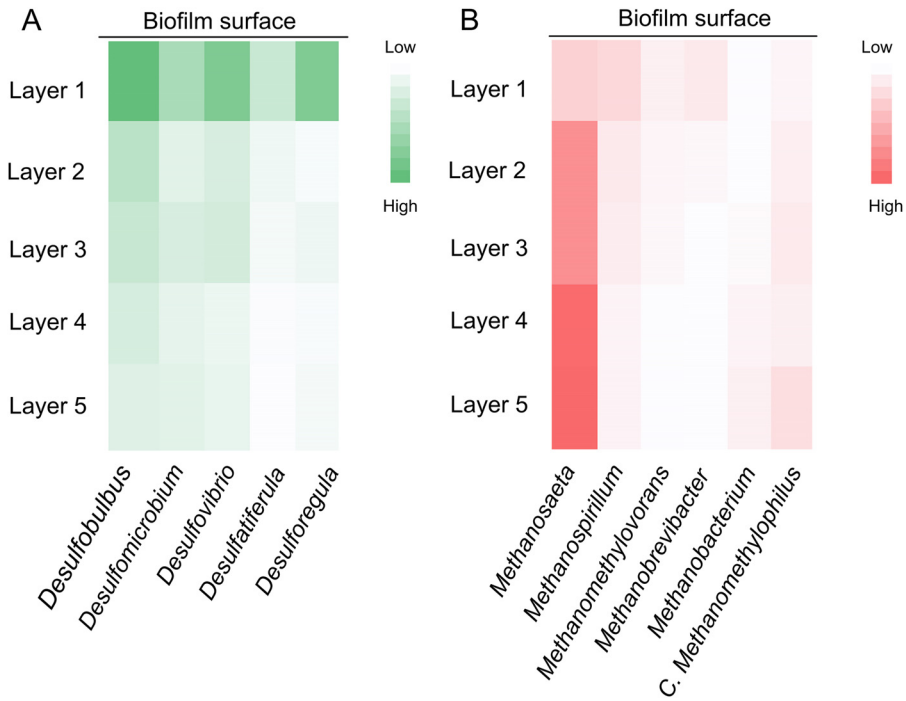

FIG 6 Heat map displaying the distribution of the predominant SRB (A) and MA (B) in different biofilm layers from the biofilm surface to the bottom (Layer 1 to Layer 5).

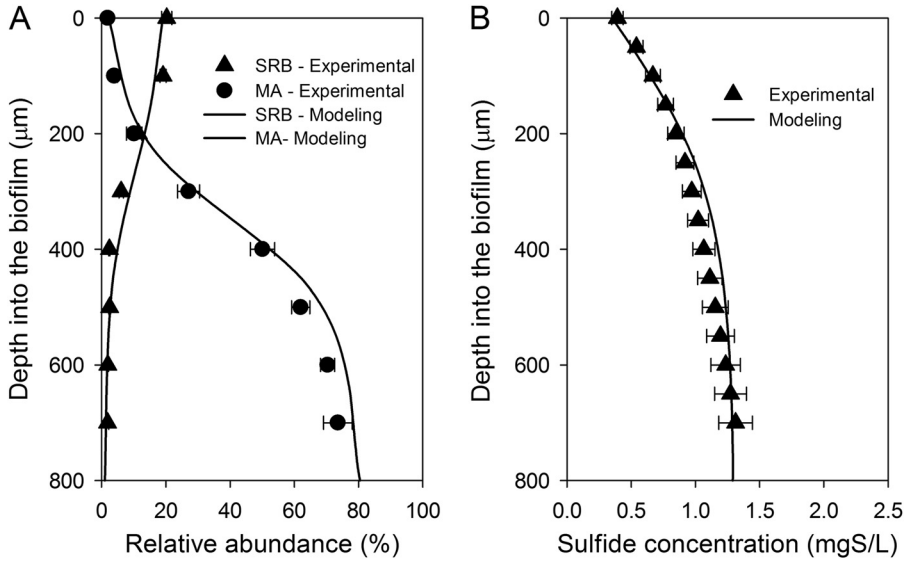

FIG 7 Comparison of model-predicted results with the experimentally measured data. (A) Relative abundances of SRB and MA. (B) Sulfide concentration profiles in the biofilm.

chemicals added for in-sewer sulfide and methane mitigation. Jiang et al. (45) found that sewer biofilms were capable of methanogenesis after nitrate dosing for 4 weeks. To explain this, they suggested that nitrate was not able to fully penetrate into the biofilm and that it failed to reach the MA in the deeper layer. This suggestion is supported by results showing a complete suppression of methane production after they increased the nitrate-dosing rate. Similar results were also observed by Ganigué et al. (46), where they found that methane was produced by the sewer biofilms after oxygen treatment and attributed that production to the partial penetration of oxygen. Consequently, given the spatial distribution of MA in sewer biofilms, full penetration of chemicals into biofilms is required to completely control methane production. This should be an important consideration for methane abatement strategies in sewers. Due to the difficulty in obtaining intact biofilm from real sewers, it remains to be verified whether the biofilm developed in our laboratory reactor fully represents that in real sewers, despite the use of realistic wastewater and shear conditions. Therefore, the implications discussed above need to be verified in real sewer systems.

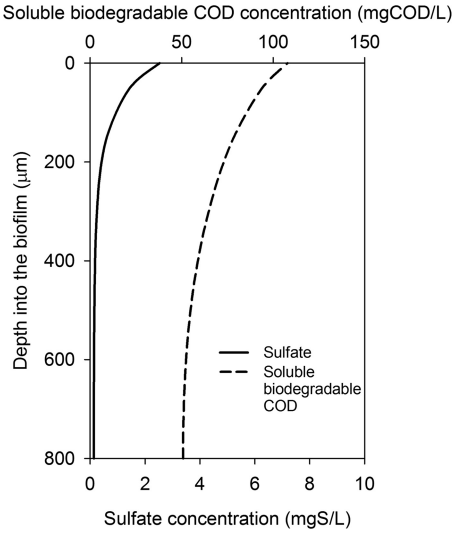

FIG 8 Model-predicted sulfate and soluble biodegradable COD profiles in the biofilm.

Phylogenic diversities of SRB and MA and their hypothesized functions. This study innovatively used pyrosequencing coupled with cryosectioning to investigate the phylogenetic diversity of SRB and MA in anaerobic sewer biofilms. Pyrosequencing can provide phylogenetic information that is more detailed than that provided by FISH. Together with cryosectioning, the phylogenetic characteristics at different depths in the biofilms were investigated. However, note that, due to the significant quantity of biomass required for pyrosequencing analysis, the biofilm sections needed for this purpose were much thicker than those needed for FISH (150 μm versus 10 μm in this study). Consequently, the spatial resolution of the method was limited to layers of this size. However, this approach was successful and revealed the microbial diversity of both SRB and MA at five depths of the biofilm, allowing us to attempt to reconstruct the possible metabolic transformations in different regions of the sewer biofilm.

SRB detected in this anaerobic sewer biofilm were mainly affiliated with five genera: *Desulfobulbus*, *Desulfovibrio*, *Desulfomicrobium*, *Desulforegula*, and *Desulfatiferula*. The first four of those genera have also been found in aerobic and anoxic wastewater biofilms, with *Desulfobulbus*, *Desulfovibrio*, and *Desulfomicrobium* appearing in higher abundances (2, 14, 47, 48). Also, *Desulfobulbus* and *Desulfovibrio* are reported to be numerically important in anaerobic methanogenic-sulfidogenic aggregates (40). *Desulfatiferula* is a genus that was newly defined by Cravo-Laureau et al. (49), and members are mesophilic, Gram-negative sulfate-reducing bacteria.

SRB can use many different compounds besides acetate and hydrogen as electron acceptors (37, 50, 51). Among the bacteria in the studied sewer biofilm, *Desulfobulbus* spp., with 98.4% sequence identity to *Desulfobulbus propionicus*, are well-known pro-

pionate-utilizing SRB (2, 51, 52). As SRB tend to out-compete acetogenic bacteria for propionate utilization due to their stronger affinity for this carbon substrate (36, 53), the high fraction of *Desulfobulbus* in the SRB population explained the low propionate concentration (<1 mg COD/liter) in the effluent. *Desulfovibrio* spp. can use hydrogen, formate, lactate, pyruvate, and many other organic compounds to reduce sulfate (54). It has been suggested that *Desulfovibrio* is an important member of the hydrogen-utilizing bacteria in wastewater biofilms (2, 48). *Desulfomicrobium* spp. are also able to use various substrates such as hydrogen, acetate, and lactate (55, 56). It is recognized that hydrogen, acetate, and propionate are important electron donors for sulfate reduction in sewer systems (33, 34). However, in this study, we also observed the proliferation of SRB, which normally use on large-molecule organic substrates rather than on hydrogen, acetate, and propionate for growth. *Desulforegula* and *Desulfatiferula* are known to use long-chain fatty acids and long-chain alkenes to reduce sulfate (49, 57). Also, some *Desulfovibrio* spp. are known to use amino acids and many other organic compounds as electron donors (54, 58). It is thought that SRB can be out-competed by very-fast-growing fermentative (acidogenic) bacteria for the large-molecule organic substrates (50, 59). However, since fermentable COD or sCOD is abundant in sewer systems and they would not be totally used by fermentative bacteria (Fig. 8), the coexistence of SRB using large-molecule organic substrates with fast-growing fermentative bacteria is possible. From an ecological viewpoint, it would be interesting to understand how different SRB, which use different electron donors, compete for sulfate when it is limiting. However, to date, only a few studies have addressed this competition for sulfate (51). The coexistence of different SRB in our biofilm seems to indicate that their affinities to sulfate are similar.

Though SRB mainly inhabited the outer layer of the sewer biofilm, small amounts of *Desulfobulbus*, *Desulfomicrobium*, and *Desulfovibrio* were also observed in the inner layers (Fig. 6). Since sulfate did not penetrate here, the SRB in the inner layers probably grew by fermenting organic matter. *Desulfobulbus* species can ferment lactate and ethanol (plus carbon dioxide) to acetate and propionate in the absence of sulfate, and many *Desulfovibrio* and *Desulfomicrobium* species grow by fermenting pyruvate to form acetate, carbon dioxide, and hydrogen as products (51, 54, 55). In comparison, *Desulforegula* and *Desulfatiferula* were not detected in the inner layers, as the ability of these SRB to ferment organic matter is limited (49, 57).

Of the MA, about 90% of the population was *Methanosaeta*, which is an obligate acetoclastic methanogen. Therefore, acetate was likely the main substrate for methanogenesis in anaerobic sewer systems. Since acetate could be simultaneously produced and consumed in the sewer system, the accumulation of acetate is probably due to the production rate of acetate being higher than its consumption rate under the tested conditions. Currently, the only genera known to use acetate for methanogenesis are *Methanosarcina* and *Methanosaeta*. However, *Methanosarcina* failed to inhabit in the anaerobic sewer biofilms, which is consistent with the finding that usually only one acetoclastic methanogen dominates such anaerobic environments (60). It is likely that *Methanosaeta* out-competed *Methanosarcina* due to differences in their affinities for acetate. *Methanosaeta* is a superior acetate utilizer in that it can use acetate at concentrations as low as 5 to 20 μM, while *Methanosarcina* requires a minimum concentration of about 1 mM (61). The acetate concentration in the wastewater was about 0.6 mM and would therefore not favor the growth of *Methanosarcina*.

MA that use other substrates such as hydrogen or methylated compounds accounted for only less than 10% of the total MA population in the sewer biofilm. The hydrogen-utilizing MA mainly belonged to genera of *Methanobrevibacter*, *Methanospirillum*, and *Methanobacterium*. Theoretically, the relative contributions of acetate and hydrogen in methanogenesis are close to 2:1, given the fact that the fermentation of hexose yields 4 H_2, 2 acetate, and 2 CO_2 and that 4 H_2 are required to reduce CO_2 to methane (62). One possible reason for the low abundance of hydrogenotrophic MA in the sewer biofilms was the low hydrogen concentration in the system. This can be explained by the fact that hydrogenotrophic MA were out-competed by the hydrogen-utilizing SRB, which have higher affinity and lower threshold values for hydrogen (35, 36). In addition, at 20°C, homoacetogenesis might occur, which could also out-compete methanogenesis for hydrogen (63). It is interesting that, although there were more SRB in the outer layer of the biofilm, the hydrogen-utilizing MA were more abundant in the outer layer than in the inner layers (Fig. 6). Though hydrogen was largely consumed by SRB, still more hydrogen was available in the outer layer, due to H_2-producing bacteria having a higher abundance in the outer layer (data not shown). *Methanomethylovorans* and "*Candidatus* Methanomethylophilus" are known to use methylated compounds such as methanol, methanethiol, and dimethyl sulfide for methanogenesis (64–66). Their low abundance could be explained by the relatively low concentrations of these substrates in the wastewater (67, 68).

ACKNOWLEDGMENTS

This research received support from the Australian Research Council, DC Water (United States), Gold Coast City Council, Melbourne Water Corporation, South East Water Limited, and Western Australia Water Corporation under project LP110201095. Keshab Raj Sharma and Zhiguo Yuan acknowledge support by the CRC for Water Sensitive Cities Pty. Ltd. Bing-Jie Ni acknowledges the support of an Australian Research Council Discovery Early Career Researcher Award (DE130100451). Jing Sun acknowledges scholarship support from the Chinese Scholarship Council.

We acknowledge Yang Lu for the help with pyrosequencing analysis and Ursula Werner for the help with microelectrode analyses.

REFERENCES

1. **Hvitved-Jacobsen T.** 2002. Sewer processes: microbial and chemical process engineering of sewer networks. CRC Press, Boca Raton, FL.
2. **Okabe S, Ito T, Satoh H.** 2003. Sulfate-reducing bacterial community structure and their contribution to carbon mineralization in a wastewater biofilm growing under microaerophilic conditions. Appl. Microbiol. Biotechnol. **63:**322–334. http://dx.doi.org/10.1007/s00253-003-1395-3.
3. **Jiang G, Gutierrez O, Sharma KR, Yuan Z.** 2010. Effects of nitrite concentration and exposure time on sulfide and methane production in sewer systems. Water Res. **44:**4241–4251. http://dx.doi.org/10.1016/j.watres.2010.05.030.
4. **Vollertsen J, Nielsen AH, Jensen HS, Wium-Andersen T, Hvitved-Jacobsen T.** 2008. Corrosion of concrete sewers—the kinetics of hydrogen sulfide oxidation. Sci. Total Environ. **394:**162–170. http://dx.doi.org/10.1016/j.scitotenv.2008.01.028.
5. **Jiang G, Wightman E, Donose BC, Yuan Z, Bond PL, Keller J.** 2014. The role of iron in sulfide induced corrosion of sewer concrete. Water Res. **49:**166–174. http://dx.doi.org/10.1016/j.watres.2013.11.007.
6. **Ganigue R, Gutierrez O, Rootsey R, Yuan Z.** 2011. Chemical dosing for sulfide control in Australia: an industry survey. Water Res. **45:**6564–6574. http://dx.doi.org/10.1016/j.watres.2011.09.054.
7. **Boon AG.** 1995. Septicity in sewers—causes, consequences and containment. Water Sci. Technol. **31:**237–253.

8. **Foley J, Yuan Z, Lant P.** 2009. Dissolved methane in rising main sewer system: field measurement and simple model development for estimating greenhouse gas emission. Water Sci. Technol. **60:**2963–2971. http://dx.doi.org/10.2166/wst.2009.718.
9. **Guisasola A, de Haas D, Keller J, Yuan Z.** 2008. Methane formation in sewer systems. Water Res. **42:**1421–1430. http://dx.doi.org/10.1016/j.watres.2007.10.014.
10. **Global Water Research Coalition (GWRC).** 2011. N_2O and CH_4 emission from wastewater collection and treatment systems—technical report. Global Water Research Coalition, London, United Kingdom.
11. **Lovley DR, Dwyer DF, Klug MJ.** 1982. Kinetic analysis of competition between sulfate reducers and methanogens for hydrogen in sediments. Appl. Environ. Microbiol. **43:**1373–1379.
12. **Schönheit P, Kristjansson JK, Thauer RK.** 1982. Kinetic mechanism for the ability of sulfate reducers to out-compete methanogens for acetate. Arch. Microbiol. **132:**285–288. http://dx.doi.org/10.1007/BF00407967.
13. **Raskin L, Rittmann B, Stahl D.** 1996. Competition and coexistence of sulfate-reducing and methanogenic populations in anaerobic biofilms. Appl. Environ. Microbiol. **62:**3847–3857.
14. **Ito T, Nielsen JL, Okabe S, Watanabe Y, Nielsen PH.** 2002. Phylogenetic identification and substrate uptake patterns of sulfate-reducing bacteria inhabiting an oxic-anoxic sewer biofilm determined by combining microautoradiography and fluorescent in situ hybridization. Appl. Environ. Microbiol. **68:**356–364. http://dx.doi.org/10.1128/AEM.68.1.356-364.2002.
15. **Damgaard LR, Nielsen LP, Revsbech NP.** 2001. Methane microprofiles in a sewage biofilm determined with a microscale biosensor. Water Res. **35:**1379–1386. http://dx.doi.org/10.1016/S0043-1354(00)00412-7.
16. **Lücker S, Steger D, Kjeldsen KU, MacGregor BJ, Wagner M, Loy A.** 2007. Improved 16S rRNA-targeted probe set for analysis of sulfate-reducing bacteria by fluorescence in situ hybridization. J. Microbiol. Methods **69:**523–528. http://dx.doi.org/10.1016/j.mimet.2007.02.009.
17. **Enfinger KL, Mitchell PS.** 2010. Scattergraph principles and practice: evaluating self-cleansing in existing sewers using the tractive force method, p 4458–4467. Abstr. World Environ. Water Resour. Congr. http://dx.doi.org/10.1061/41114(371)453.
18. **Sutherland-Stacey L, Corrie S, Neethling A, Johnson I, Gutierrez O, Dexter R, Yuan Z, Keller J, Hamilton G.** 2008. Continuous measurement of dissolved sulfide in sewer systems. Water Sci. Technol. **57:**375–381. http://dx.doi.org/10.2166/wst.2008.132.
19. **Kühl M, Jørgensen BB.** 1992. Microsensor measurements of sulfate reduction and sulfide oxidation in compact microbial communities of aerobic biofilms. Appl. Environ. Microbiol. **58:**1164–1174.
20. **Gutierrez O, Mohanakrishnan J, Sharma KR, Meyer RL, Keller J, Yuan ZG.** 2008. Evaluation of oxygen injection as a means of controlling sulfide production in a sewer system. Water Res. **42:**4549–4561. http://dx.doi.org/10.1016/j.watres.2008.07.042.
21. **Gieseke A, de Beer D.** 2004. Section 8 update: use of microelectrodes to measure in situ microbial activities in biofilms, sediments, and microbial mats, p 3483–3514. *In* Kowalchuk GA, de Bruijn FJ, Head IM, Akkermans AD, van Elsas JD (ed), Molecular microbial ecology manual. Springer, Dordrecht, the Netherlands.
22. **Loy A, Maixner F, Wagner M, Horn M.** 2007. probeBase—an online resource for rRNA-targeted oligonucleotide probes: new features 2007. Nucleic Acids Res. **35:**D800–D804. http://dx.doi.org/10.1093/nar/gkl856.
23. **Crocetti G, Murto M, Bjornsson L.** 2006. An update and optimisation of oligonucleotide probes targeting methanogenic Archaea for use in fluorescence in situ hybridisation (FISH). J. Microbiol. Methods **65:**194–201. http://dx.doi.org/10.1016/j.mimet.2005.07.007.
24. **Batstone DJ, Keller J, Blackall LL.** 2004. The influence of substrate kinetics on the microbial community structure in granular anaerobic biomass. Water Res. **38:**1390–1404. http://dx.doi.org/10.1016/j.watres.2003.12.003.
25. **Amann RI, Krumholz L, Stahl DA.** 1990. Fluorescent-oligonucleotide probing of whole cells for determinative, phylogenetic, and environmental studies in microbiology. J. Bacteriol. **172:**762–770.
26. **Daims H, Lucker S, Wagner M.** 2006. Daime, a novel image analysis program for microbial ecology and biofilm research. Environ. Microbiol. **8:**200–213. http://dx.doi.org/10.1111/j.1462-2920.2005.00880.x.
27. **Amann RI, Ludwig W, Schleifer KH.** 1995. Phylogenetic identification and in-situ detection of individual microbial cells without cultivation. Microbiol. Rev. **59:**143–169.
28. **Caporaso JG, Kuczynski J, Stombaugh J, Bittinger K, Bushman FD, Costello EK, Fierer N, Pena AG, Goodrich JK, Gordon JI, Huttley GA, Kelley ST, Knights D, Koenig JE, Ley RE, Lozupone CA, McDonald D, Muegge BD, Pirrung M, Reeder J, Sevinsky JR, Tumbaugh PJ, Walters WA, Widmann J, Yatsunenko T, Zaneveld J, Knight R.** 2010. QIIME allows analysis of high-throughput community sequencing data. Nat. Methods **7:**335–336. http://dx.doi.org/10.1038/nmeth.f.303.
29. **Bragg L, Stone G, Imelfort M, Hugenholtz P, Tyson GW.** 2012. Fast, accurate error-correction of amplicon pyrosequences using acacia. Nat. Methods **9:**425–426. http://dx.doi.org/10.1038/nmeth.1990.
30. **Wu ST, Zhu ZW, Fu LM, Niu BF, Li WZ.** 7 September 2011. WebMGA: a customizable web server for fast metagenomic sequence analysis. BMC Genomics **12:**444. http://dx.doi.org/10.1186/1471-2164-12-444.
31. **Caporaso JG, Bittinger K, Bushman FD, DeSantis TZ, Andersen GL, Knight R.** 2010. Pynast: a flexible tool for aligning sequences to a template alignment. Bioinformatics **26:**266–267. http://dx.doi.org/10.1093/bioinformatics/btp636.
32. **Reichert P.** 1994. AQUASIM—a tool for simulation and data analysis of aquatic systems. Water Sci. Technol. **30:**21–30.
33. **Sharma KR, Yuan Z, de Haas D, Hamilton G, Corrie S, Keller J.** 2008. Dynamics and dynamic modelling of H_2S production in sewer systems. Water Res. **42:**2527–2538. http://dx.doi.org/10.1016/j.watres.2008.02.013.
34. **Guisasola A, Sharma KR, Keller J, Yuan Z.** 2009. Development of a model for assessing methane formation in rising main sewers. Water Res. **43:**2874–2884. http://dx.doi.org/10.1016/j.watres.2009.03.040.
35. **Kristjansson JK, Schonheit P, Thauer RK.** 1982. Different K_s values for hydrogen of methanogenic bacteria and sulfate reducing bacteria—an explanation for the apparent inhibition of methanogenesis by sulfate. Arch. Microbiol. **131:**278–282. http://dx.doi.org/10.1007/BF00405893.
36. **Uberoi V, Bhattacharya SK.** 1997. Sulfate-reducing bacteria in anaerobic propionate systems. J. Environ. Eng. (New York) **123:**675–682.
37. **Kalyuzhnyi SV, Fedorovich VV.** 1998. Mathematical modelling of competition between sulphate reduction and methanogenesis in anaerobic reactors. Bioresour. Technol. **65:**227–242. http://dx.doi.org/10.1016/S0960-8524(98)00019-4.
38. **Nielsen PH.** 1987. Biofilm dynamics and kinetics during high-rate sulfate reduction under anaerobic conditions. Appl. Environ. Microbiol. **53:**27–32.
39. **Yoda M, Kitagawa M, Miyaji Y.** 1987. Long term competition between sulfate-reducing and methane-producing bacteria for acetate in anaerobic biofilm. Water Res. **21:**1547–1556. http://dx.doi.org/10.1016/0043-1354(87)90140-0.
40. **Santegoeds CM, Damgaard LR, Hesselink G, Zopfi J, Lens P, Muyzer G, de Beer D.** 1999. Distribution of sulfate-reducing and methanogenic bacteria in anaerobic aggregates determined by microsensor and molecular analyses. Appl. Environ. Microbiol. **65:**4618–4629.
41. **Hilton B, Oleszkiewicz J.** 1988. Sulfide-induced inhibition of anaerobic digestion. J. Environ. Eng. **114:**1377–1391. http://dx.doi.org/10.1061/(ASCE)0733-9372(1988)114:6(1377).
42. **Parkin GF, Lynch NA, Kuo WC, Vankeuren EL, Bhattacharya SK.** 1990. Interaction between sulfate reducers and methanogens fed acetate and propionate. J. Water Pollut. Control Fed. **62:**780–788.
43. **Harmsen HJ, Kengen HM, Akkermans AD, Stams AJ, de Vos WM.** 1996. Detection and localization of syntrophic propionate-oxidizing bacteria in granular sludge by in situ hybridization using 16S rRNA-based oligonucleotide probes. Appl. Environ. Microbiol. **62:**1656–1663.
44. **O'Flaherty V, Mahony T, O'Kennedy R, Colleran E.** 1998. Effect of pH on growth kinetics and sulphide toxicity thresholds of a range of methanogenic, syntrophic and sulphate-reducing bacteria. Process Biochem. **33:**555–569. http://dx.doi.org/10.1016/S0032-9592(98)00018-1.
45. **Jiang G, Sharma KR, Yuan Z.** 2013. Effects of nitrate dosing on methanogenic activity in a sulfide-producing sewer biofilm reactor. Water Res. **47:**1783–1792. http://dx.doi.org/10.1016/j.watres.2012.12.036.
46. **Ganigué R, Yuan Z.** 2014. Impact of oxygen injection on CH_4 and N_2O emissions from rising main sewers. J. Environ. Manage. **144:**279–285. http://dx.doi.org/10.1016/j.jenvman.2014.04.023.
47. **Okabe S, Itoh T, Satoh H, Watanabe Y.** 1999. Analyses of spatial distributions of sulfate-reducing bacteria and their activity in aerobic wastewater biofilms. Appl. Environ. Microbiol. **65:**5107–5116.
48. **Ito T, Okabe S, Satoh H, Watanabe Y.** 2002. Successional development of sulfate-reducing bacterial populations and their activities in a wastewater biofilm growing under microaerophilic conditions. Appl. Environ. Microbiol. **68:**1392–1402. http://dx.doi.org/10.1128/AEM.68.3.1392-1402.2002.

49. **Cravo-Laureau C, Labat C, Joulian C, Matheron R, Hirschler-Réa A.** 2007. Desulfatiferula olefinivorans gen. nov., sp. nov., a long-chain n-alkene-degrading, sulfate-reducing bacterium. Int. J. Syst. Evol. Microbiol. **57:**2699–2702. http://dx.doi.org/10.1099/ijs.0.65240-0.
50. **Fedorovich V, Lens P, Kalyuzhnyi S.** 2003. Extension of anaerobic digestion model no. 1 with processes of sulfate reduction. Appl. Biochem. Biotechnol. **109:**33–45. http://dx.doi.org/10.1385/ABAB:109:1-3:33.
51. **Muyzer G, Stams AJM.** 2008. The ecology and biotechnology of sulphate-reducing bacteria. Nat. Rev. Microbiol. **6:**441–454. http://dx.doi.org/10.1038/nrmicro1892.
52. **Pagani I, Lapidus A, Nolan M, Lucas S, Hammon N, Deshpande S, Cheng JF, Chertkov O, Davenport K, Tapia R, Han C, Goodwin L, Pitluck S, Liolios K, Mavromatis K, Ivanova N, Mikhailova N, Pati A, Chen A, Palaniappan K, Land M, Hauser L, Chang YJ, Jeffries CD, Detter JC, Brambilla E, Kannan KP, Djao ODN, Rohde M, Pukall R, Spring S, Goker M, Sikorski J, Woyke T, Bristow J, Eisen JA, Markowitz V, Hugenholtz P, Kyrpides NC, Klenk HP.** 2011. Complete genome sequence of Desulfobulbus propionicus type strain (1pr3^T). Stand. Genomic Sci. **4:**100–110. http://dx.doi.org/10.4056/sigs.1613929.
53. **Rinzema A, Lettinga G.** 1988. Anaerobic treatment of sulfate containing waste water, p 65–109. *In* Wise DL (ed), Biotreatment systems, vol III. CRC Press, Boca Raton, FL.
54. **Voordouw G.** 1995. The genus Desulfovibrio: the centennial. Appl. Environ. Microbiol. **61:**2813–2819.
55. **Barton LL, Fauque GD.** 2009. Biochemistry, physiology and biotechnology of sulfate-reducing bacteria. Adv. Appl. Microbiol. **68:**41–98. http://dx.doi.org/10.1016/S0065-2164(09)01202-7.
56. **Dias M, Salvado JC, Monperrus M, Caumette P, Amouroux D, Duran R, Guyoneaud R.** 2008. Characterization of Desulfomicrobium salsuginis sp. nov. and Desulfomicrobium aestuarii sp. nov., two new sulfate-reducing bacteria isolated from the Adour estuary (French Atlantic coast) with specific mercury methylation potentials. Syst. Appl. Microbiol. **31:**30–37. http://dx.doi.org/10.1016/j.syapm.2007.09.002.
57. **Rees GN, Patel BKC.** 2001. Desulforegula conservatrix gen. nov., sp. nov., a long-chain fatty acid-oxidizing, sulfate-reducing bacterium isolated from sediments of a freshwater lake. Int. J. Syst. Evol. Microbiol. **51:**1911–1916. http://dx.doi.org/10.1099/00207713-51-5-1911.
58. **Hernandez-Eugenio G, Fardeau ML, Patel BKC, Macarie H, Garcia JL, Ollivier B.** 2000. Desulfovibrio mexicanus sp. nov., a sulfate-reducing bacterium isolated from an upflow anaerobic sludge blanket (uasb) reactor treating cheese wastewaters. Anaerobe **6:**305–312. http://dx.doi.org/10.1006/anae.2000.0354.
59. **Widdel F.** 1988. Microbiology and ecology of sulfate- and sulphur-reducing bacteria, p 469–585. *In* Zehnder AJB (ed), Biology of anaerobic microorganisms. Wiley, New York, NY.
60. **Leclerc M, Delgenes JP, Godon JJ.** 2004. Diversity of the archaeal community in 44 anaerobic digesters as determined by single strand conformation polymorphism analysis and 16S rDNA sequencing. Environ. Microbiol. **6:**809–819. http://dx.doi.org/10.1111/j.1462-2920.2004.00616.x.
61. **Jetten MSM, Stams AJM, Zehnder AJB.** 1992. Methanogenesis from acetate—a comparison of the acetate metabolism in Methanothrix soehngenii and Methanosarcina spp. FEMS Microbiol. Lett. **88:**181–197. http://dx.doi.org/10.1111/j.1574-6968.1992.tb04987.x.
62. **Liu Y, Whitman WB.** 2008. Metabolic, phylogenetic, and ecological diversity of the methanogenic archaea. Ann. N. Y. Acad. Sci. **1125:**171–189. http://dx.doi.org/10.1196/annals.1419.019.
63. **Conrad R, Bak F, Seitz HJ, Thebrath B, Mayer HP, Schutz H.** 1989. Hydrogen turnover by psychrotrophic homoacetogenic and mesophilic methanogenic bacteria in anoxic paddy soil and lake sediment. FEMS Microbiol. Ecol. **62:**285–294. http://dx.doi.org/10.1111/j.1574-6968.1989.tb03382.x.
64. **Borrel G, Harris HMB, Toney W, Mihajlovski A, Parisot N, Peyretaillade E, Peyret P, Gribaldo S, O'Toole PW, Brugere JF.** 2012. Genome sequence of "Candidatus Methanomethylophilus alvus" Mx1201, a methanogenic archaeon from the human gut belonging to a seventh order of methanogens. J. Bacteriol. **194:**6944–6945. http://dx.doi.org/10.1128/JB.01867-12.
65. **Cha IT, Min UG, Kim SJ, Yim KJ, Roh SW, Rhee SK.** 2013. Methanomethylovorans uponensis sp. nov., a methylotrophic methanogen isolated from wetland sediment. Antonie Van Leeuwenhoek **104:**1005–1012. http://dx.doi.org/10.1007/s10482-013-0020-4.
66. **Lomans BP, Maas R, Luderer R, den Camp H, Pol A, van der Drift C, Vogels GD.** 1999. Isolation and characterization of Methanomethylovorans hollandica gen. nov., sp. nov., isolated from freshwater sediment, a methylotrophic methanogen able to grow on dimethyl sulfide and methanethiol. Appl. Environ. Microbiol. **65:**3641–3650.
67. **Sun J, Hu S, Sharma KR, Keller-Lehmann B, Yuan Z.** 2014. An efficient method for measuring dissolved VOSCs in wastewater using GC-SCD with static headspace technique. Water Res. **52:**208–217. http://dx.doi.org/10.1016/j.watres.2013.10.063.
68. **Hwang Y, Matsuo T, Hanaki K, Suzuki N.** 1995. Identification and quantification of sulfur and nitrogen containing odorous compounds in wastewater. Water Res. **29:**711–718. http://dx.doi.org/10.1016/0043-1354(94)00145-W.